Zhang, J., Huang, B., Shao, Q., & Huang, X. (2018). Highly active, selective, and stable direct H2O2 generation by monodispersive Pd–Ag nanoalloy. ACS applied materials & interfaces, 10(25), 21291-21296.

Highly Active, Selective, and Stable Direct H_2O_2 Generation by Monodispersive Pd-Ag Nanoalloy

Jin Zhang, Qi Shao, Pengtang Wang, Bolong Huang, Shuxing Bai and Xiaoqing Huang**

ABSTRACT: The H_2O_2 is an oxidant has wide applications in industrial chemical synthesis, and also a candidate to replace the traditional oxidants such as chloride-based strong acids etc. The direct synthesis of H_2O_2 from H_2 and O_2 is promsing industrial technology as it is a green and atomically economic reaction. However, the conventional Pd-based routes are notorious in complicated post-purification procdures, high energy costs, and low selectivities due to large energy trend towards O-O bond cleavage. We have solved this problem by tuning oxidation state of Pd with high-activity remained via a wet-chemical synthesis of binary monodisperse Pd-Ag nanoalloy (NA) with flexibly tuned size and composition.. The catalysts show outstanding stability with negligible productivity and selectivity degradations over consecutive runs. Both the X-ray photoelectron spectroscopy analysis and theoretical calculation confirm the electron transfer from Ag to Pd, which generates more Pd^0 and enables improved H_2O_2 productivity. We have demonstrated that the incorporation of Ag is of importance for enhancing the performance of Pd-Ag NA for the direct H_2O_2 synthesis with preservations of O_2^{2-} and efficiently cleavage H^+. Additionally, the enhanced H_2O_2 desorption on the PdAg NPs is beneficial for releasing H_2O_2 from the surface, which results in the increased H_2O_2 selectivity.

Hydrogen peroxide (H_2O_2), listed as one of one hundred most important chemicals in the world, has drawn much research attention due to its high energy efficiency and the feature of clean.[1-3] Until now, many synthesis processes of H_2O_2 have been investigated, such as: anthraquinone autoxidation,[4,5] electrochemical synthesis[6-7] and photocatalytic synthesis.[8-

[*] J. Zhang, Q. Shao, P. Wang, S. Bai, Prof. X. Huang
College of Chemistry, Chemical Engineering and Materials Science, Soochow University, Jiangsu 215123, China.
E-mail: hxq006@suda.edu.cn

[*] Dr. B. Huang, Department of Applied Biology and Chemical Technology, The Hong Kong Polytechnic University, Hung Hom, Kowloon, Hong Kong SAR, China.
E-mail: bhuang@polyu.edu.hk

[**] This work was financially supported by the Ministry of Science and Technology (2016YFA0204100, 2017YFA0208200), the National Natural Science Foundation of China (21571135), Young Thousand Talented Program, the start-up supports from Soochow University, and the Priority Academic Program Development of Jiangsu Higher Education Institutions (PAPD).

Supporting information for this article is available on the WWW under http://www.angewandte.org or from the author.

[10] While the anthraquinone process is the major industrial H_2O_2 production process, due to its safety and easy to continuous running, the energy waste is brought by the purification of the reaction substrate and the expensive operating cost, which become the major challenge to the large-scale application.[11-13] Due to the distinct advantages of atom economy, lower energy consumption and only by-product of H_2O, the direct synthesis of H_2O_2 has become a promising process to the production of H_2O_2.[2, 14,15] The formidable challenge of the direct H_2O_2 synthesis is to realize high H_2O_2 selectivity and prevent H_2O formation from the excessive H_2O_2 hydrogenation simultaneously [16,17].

Previous studies have indicated that Pd-based materials are the most active catalysts to the direct H_2O_2 synthesis.[15, 18-20] To further improve the H_2O_2 selectivity, a number of Pd-based catalysts have been investigated by adding extra acid and halide promoters, which however largely increased the difficulty to the purification of subsequent products.[13,21] Another strategy is ligand-modified hybrid catalyst with enhanced performance, but the selectivity can be rapidly decreased due to the leaching of the organic ligand.[15, 22] In fact, several previous studies have shown that the introduction of the second metal to Pd-based catalyst would be a promising strategy to enhance the direct H_2O_2 synthesis.[23-25] Considering that the oxidizable Ag can transfer electron to Pd to maintain the Pd^0 species as the active sites for the direct H_2O_2 synthesis, the bimetallic Pd-Ag alloy can be a promising candidate for the direct H_2O_2 synthesis.[26,27]

Herein, we synthesized a class of monodisperse PdAg alloy NPs with high activity and favorable selectivity towards the direct H_2O_2 synthesis. With tuning the amounts of metal precursor and dodecyltrimethylammonium chloride (DTAC), three different components of Pd-Ag alloy NPs (denoted as: PdAg, $Pd_{1.5}Ag$, and $PdAg_{1.5}$, respectively) and the other three different sizes of Pd-Ag alloy NPs (the NPs sizes from small to medium and large were denoted as PdAg-S, PdAg-M, PdAg-L, respectively) were obtained. By tuning the catalytic parameters, the optimized PdAg-M NPs exhibited high H_2O_2 productivity of 80.4 mol kg_{cat}^{-1} h^{-1}, low H_2O_2 hydrogenation activity of 30.0 mol kg_{cat}^{-1} h^{-1} and desirable selectivity of 82.1%, much better than those of Ag NPs, Pd NPs as well as the commercial Pd/C. The PdAg-M NPs also exhibited high stability with negligible productivity and selectivity degradations after six rounds. The theoretical calculation demonstrated that the PdAg alloy surface had the charge transfer from Ag to Pd and showed more energetically preference for the H_2O_2 synthesis than Pd surface, in line with the X-ray photoelectron spectroscopy (XPS) results. In addition, the enhanced H_2O_2

desorption on the PdAg alloy surface is beneficial for releasing the H_2O_2 molecules from the surface, which results in the increased H_2O_2 selectivity.

The PdAg alloy NPs were synthesized through a simple wet-chemical method, where silver (I) acetate (AgAc), palladium (II) acetylacetonate ($Pd(acac)_2$), benzoin, DTAC and oleylamine (OAm) were added into a vial and immerged in an oil bath of 140 ºC for 5 h (see the supporting information for details). The high-angle annular dark-field scanning transmission electron microscopy images (HAADF-STEM, **Figure 1a,b**) showed that the obtained NPs had high uniformity and excellent dispersibility. The Pd/Ag atomic ratio was determined to be 49.2/50.8, as confirmed by scanning electron microscopy energy-dispersive X-ray spectroscopy (SEM-EDS, **Figure 1c**), which fairly closed the feeding ratio of metal precursors. The X-ray diffraction (XRD) pattern of PdAg-M NPs (**Figure 1d**) had a set of peaks at around 38.87º, 45.93º, 66.18º, and 79.15º, respectively, which were between the peaks of Ag (JCPDS no.04-0783) and Pd (JCPDS no.46-1043), indicating that the PdAg-M NPs had alloy phase.[28,29] The high resolution TEM (HRTEM, **Figure 1e**) of the PdAg-M NPs was further carried out, where the 0.230 nm spacing between the d-spacing of Ag (111) crystal plane (0.236 nm) and the d-spacing of Pd (111) crystal plane (0.225 nm) was observed. The alloy feature of the obtained PdAg NPs was further demonstrated by STEM line scan analysis (**Figure 1f**) and HAADF-STEM image and corresponding element mappings analysis (**Figure 1g**), where the elements of Pd and Ag were uniformly distributed in the NPs.

We have also obtained different sizes Pd-Ag NPs by simply tuning the amounts of DTAC supplied. As shown in **Figure S1**, 4 ± 1 nm (PdAg-S NPs), 8 ± 1 nm (PdAg-M NPs), and 10 ± 1 nm (PdAg-L NPs) PdAg NPs were obtained when the dosages of DTAC were 0 mg, 13 mg, and 39 mg, respectively. XRD patterns and EDS patterns proved that these Pd-Ag NPs with different sizes maintained alloy phases (**Figures S2&S3**). As shown in **Figure S**4, HRTEM images clearly indicated the PdAg alloyed characteristic. In addition, with using different feeding ratios of the metal precursor, the regulation of component ratios to PdAg-M alloy NPs (PdAg-M NPs, $Pd_{1.5}$Ag-M NPs, $PdAg_{1.5}$-M NPs) can be realized. Corresponding characterizations were shown in **Figures S5&S6**, where EDS patterns indicated that both the component ratios of $PdAg_{1.5}$-M NPs and $Pd_{1.5}$Ag-M NPs were nearly close to the feeding ratios of metal precursors (**Figure S5c,d**). XRD patterns and HRTEM images proved that both $PdAg_{1.5}$-M NPs and $Pd_{1.5}$Ag-M NPs had alloy phase (**Figures S5e&S6**). Hence, we successfully obtained Pd-Ag alloy NPs with three different sizes and Pd-Ag alloy NPs with

three different component ratios by simply regulating the amounts of DTAC and metal precursors introduced.

To study the catalytic performance of the obtained Pd-Ag alloy NPs, the direct H_2O_2 synthesis was performed. The impact of supports on this reaction was initially investigated. To this end, we loaded catalysts on different supports, such as TiO_2, Al_2O_3, SiO_2, CeO_2, and ZrO_2, respectively (**Figures S7&S8**).[30] Catalyst loaded on TiO_2 revealed the best catalytic performance compared with those loaded on other supports. We further compared the catalytic performances of Pd-Ag alloy NPs with different sizes and different component ratios (**Figures S9&S10**). We found that the PdAg-M NPs had both the highest productivity (80.4 mol kg_{cat}^{-1} h^{-1}) and the lowest H_2O_2 hydrogenation activity (30.0 mol kg_{cat}^{-1} h^{-1}), while other four catalysts had inferior performances (**Figure 2a,b&Table S1**). Moreover, the PdAg-M NPs also showed the highest selectivity to the direct H_2O_2 synthesis (82.1%), which was far better than other catalysts. We further investigated the impact from the loading amount (**Figure 2c**). As the Pd loading increasing from 1 wt% to 5 wt%, the productivity changed from 38.8 mol kg_{cat}^{-1} h^{-1} to 80.4 mol kg_{cat}^{-1} h^{-1} and the H_2O_2 hydrogenation activity changed from 225.5 mol kg_{cat}^{-1} h^{-1} to 30.0 mol kg_{cat}^{-1} h^{-1}. Through the above study, we can conclude that the 5 wt% PdAg-M alloy NPs showed the best catalytic performance among all the catalysts investigated.

For further comparisons, we used the commercial Pd/C, Ag NPs, and Pd NPs as catalysts to perform the direct H_2O_2 synthesis reaction while kept the other parameters constant (**Figure S11**). We found that the commercial Pd/C and Ag NPs had rather poor catalytic performances (**Table S1**). The Pd NPs exhibited a relatively high productivity (66.2 mol kg_{cat}^{-1} h^{-1}), while the H_2O_2 selectivity of the Pd NPs was quite low (31.27%). Therefore, the PdAg-M alloy NPs showed much better catalytic activity than the commercial Pd/C, Ag NPs as well as Pd NPs. Finally, the stability of the PdAg-M alloy NPs was also investigated by recycling this reaction. After six rounds, the productivity can largely keep as high as 61.6 mol kg_{cat}^{-1} h^{-1} (76.6% of the initial value). The H_2O_2 selectivity still kept as high as 71.7% (87.4% of the initial value) (**Figure 3a**). The PdAg-M alloy NPs showed excellent stability with a negligible activity degradation after six rounds. TEM image shows that the catalysts can largely maintain their structure with the similar ratio of Pd/Ag (45.6/54.4) by the SEM-EDS analysis after six rounds (**Figure 3b&Figure S12**). Therefore, the PdAg-M alloy NPs showed both excellent activity and outstanding stability for the direct H_2O_2 synthesis.

To better understand the origin for the excellent catalytic performance of Pd-Ag NPs, XPS analysis was performed to investigate the valence states and electron transfer of the Pd-Ag NPs.

Pd NPs and Ag NPs were also investigated for comparisons. As shown in **Figure 4a**, the Ag 3d binding energies of these five Pd-Ag alloy NPs were different compared with pure Ag NPs (**Figure S13a**). The binding energies of these five Pd-Ag alloy NPs were approximately 367.0 eV and 373.1 eV (corresponding to Ag^{+}), while the binding energies of pure Ag NPs were 367.5 eV and 373.6 eV (corresponding to Ag^{0}),[31] which fully indicated that electron had transfered from Ag to Pd in the Pd-Ag alloy. More interesting, we found that the PdAg-M alloy NPs had a slightly decreased binding energy of Ag^{+} (366.7 eV and 372.7 eV) compared with the other Pd-Ag alloy NPs, suggesting the higher tendency of electron transfer. Since there was the most electrons transfer from Ag to Pd, the PdAg-M alloy NPs had the largest ratio of Pd^{0}/Pd^{2+} (83.15/16.85) (**Figure 4b-f**), where the most Pd^{0} could ensure the best catalytic activity, since Pd^{0} was identified as the major active site.

To support our experimental results, the theoretical calculation was further performed. We initially built *fcc*-PdAg with replacement of 50% of occupied Pd site by Ag within unit cell of *fcc*-Pd. The band structure showed the paths along (Z, A, M, Γ, Z, R, X, and Γ) in **Figure 5a**. The full path from A→M exhibited an evident forbidden band gap for transitions from occupied valence orbitals to the conducting states, which is the parallel direction along the nearest Ag→Ag. The other directions cross the Fermi level (E_F) including the path along Ag→Pd. This indicated the charge transfer prefers Ag→Pd→Ag to Ag→Ag. The result was in accordance with the XPS analysis results. In this system, Pd site on the surface PdAg alloy can be more active than Ag because the Pd-4d orbital level was higher than the one of Ag-4d, closer to the E_F (**Figure 5b**). The 4d-orbital real-space distribution on the surfaces within the energy level around E_F (0 eV) (**Figure 5c)** implies the bonding and anti-bonding 4d-orbitals PdAg (100) were more directional than the ones seen in Pd (100). This contrast demonstrated the PdAg surface can have more selectivity than Pd surface.

In general, the energetic interval between the reacting state and the thermoneutral line (ΔG=0 eV) moderately determines the abilities of absorption and desorption of species molecules. The deeper means the stronger absorption but weakens desorption, *vice versa*. As illustrated in **Figure 5d**, the direct H_2O_2 synthesis on the PdAg (ΔG=-0.068 eV) won compared with the other system like Pd (ΔG=-3.30 eV). This arises because of the energetic contrast for the formation energy between the surfaces and the H_2O_2 molecule. The PdAg (100) surface shows much easier to continuously yield the H_2O_2. On the other hand, there may further lead to a decomposition of H_2O_2 on Pd surface. We found that the Pd-Ag local squared lattice on PdAg (100) exhibited much higher activity than the Pd (100) surface (**Figure 5e**). Such squared

local lattice could be treated as unit area to actively adsorb the H_2 and O_2 simultaneously, and further stabilized the O_2 in the diatomic molecular form. The most stable configuration for O_2 location on the PdAg (100) was the bridge-bonding with Pd and Ag for each O with the O-O bond along the diagonal line of Pd-Ag local square lattice. However, this configuration was rather unstable for H_2. The H-H would be separated apart and individually formed Pd-H-Ag bonding at the bridge-site between Pd-Ag bonding. The most stable location for the H was the hollow site on the PdAg (100) surface. Then, the two H would further intermediately evolve to the hollow site. From the **Figure 5 d**, the spontaneous charge transfer for both H and O_2 with PdAg (100) were much energetic favorable. With the Coulombic attraction, the $2H^+$ would have a fast combine with O_2^{2-} and react into the H_2O_2 finally. Based on above results, the incorporation of Ag generates the new PdAg active sites, which enhances the charge transfer (Ag→Pd) and improves the adsorption-desorption ability of surface molecules (such as H_2, O_2, H_2O_2) compared with Pd NPs. Thus the H_2O_2 selectivity is increased *via* an energetic downhill.

In summary, we have successfully synthesized Pd-Ag alloy NPs with different sizes and different Pd/Ag ratios as highly efficient catalysts for the direct H_2O_2 synthesis. The optimized PdAg-M alloy NPs show the highest performance with H_2O_2 productivity of 80.4 mol kg_{cat}^{-1} h^{-1}, H_2O_2 hydrogenation of 30.0 mol kg_{cat}^{-1} h^{-1}, and selectivity of 82.1%. The catalyst also show outstanding durability with negligible degradation after six cycles. XPS analysis demonstrates that the electron transfers from Ag to Pd to generate more Pd^0 species, which results in excellent catalytic activity. Theoretical calculation results indicate that the PdAg alloy can enhance the charge transfer from Ag to Pd and improve the adsorption-desorption ability of the surface molecules. More importantly, the new PdAg active sites have the spontaneous combination process with H and O_2 and much energetic preference to the direct H_2O_2 synthesis reaction. Our study reported here emphasize the importance of the bimetallic alloy design for the direct H_2O_2 synthesis with satisfactory efficiency.

Received: ((will be filled in by the editorial staff))
Published online on ((will be filled in by the editorial staff))

[1] Z. Zheng, Y. H. Ng, D. W. Wang, R. Amal, *Adv. Mater.* **2016**, *28*, 9949-9955.

[2] J. K. Edwards, B. Solsona, E. N. N, A. F. Carley, A. A. Herzing, C. J. Kiely, G. J. Hutchings, *Science* **2009**, *323*, 1037-1041.

[3] S. Siahrostami, A. Verdaguer-Casadevall, M. Karamad, D. Deiana, P. Malacrida, B. Wickman, M. Escudero-Escribano, E. A. Paoli, R. Frydendal, T. W. Hansen, I. Chorkendorff, I. E. Stephens, J. Rossmeisl, *Nat. Mater.* **2013**, *12*, 1137-1143.

[4] Y. Guo, C. Dai, Z. Lei, B. Chen, X. Fang, *Catal. Today* **2016**, *276*, 36-45.

[5] T. Kamachi, T. Ogata, E. Mori, K. Iura, N. Okuda, M. Nagata, K. Yoshizawa, *J. Phys. Chem. C* **2015**, *119*, 8748-8754.

[6] T. P. Fellinger, F. Hasche, P. Strasser, M. Antonietti, *J. Am. Chem. Soc.* **2012**, *134*, 4072-4075.

[7] J. S. Jirkovsky, I. Panas, E. Ahlberg, M. Halasa, S. Romani, D. J. Schiffrin, *J. Am. Chem. Soc.* **2011**, *133*, 19432-19441.

[8] Y. Shiraishi, S. Kanazawa, Y. Kofuji, H. Sakamoto, S. Ichikawa, S. Tanaka, T. Hirai, *Angew. Chem. Int. Ed.* **2014**, *53*, 13454-13459.

[9] M. Teranishi, S.-i. Naya, H. Tada, *J. Am. Chem. Soc.* **2010**, *132*, 7850-7851.

[10] D. Tsukamoto, A. Shiro, Y. Shiraishi, Y. Sugano, S. Ichikawa, S. Tanaka, T. Hirai, *ACS Catal.* **2012**, *2*, 599-603.

[11] A. Pashkova, R. Dittmeyer, *Catal. Today* **2015**, *248*, 128-137.

[12] J. K. Edwards, G. J. Hutchings, *Angew. Chem. Int. Ed.* **2008**, *47*, 9192-9198.

[13] J. García-Serna, T. Moreno, P. Biasi, M. J. Cocero, J.-P. Mikkola, T. O. Salmi, *Green Chem.* **2014**, *16*, 2320.

[14] J. Kim, Y.-M. Chung, S.-M. Kang, C.-H. Choi, B.-Y. Kim, Y.-T. Kwon, T. J. Kim, S.-H. Oh, C.-S. Lee, *ACS Catal.* **2012**, *2*, 1042-1048.

[15] G. M. Lari, B. Puértolas, M. Shahrokhi, N. López, J. Pérez-Ramírez, *Angew. Chem. Int. Ed.* **2017**, *129*, 1801-1805.

[16] J. M. Campos-Martin, G. Blanco-Brieva, J. L. Fierro, *Angew. Chem. Int. Ed.* **2006**, *45*, 6962-6984.

[17] L. Torrente-Murciano, Q. He, G. J. Hutchings, C. J. Kiely, D. Chadwick, *ChemCatChem* **2014**, *6*, 2531-2534.

[18] F. Menegazzo, M. Manzoli, M. Signoretto, F. Pinna, G. Strukul, *Catal. Today* **2015**, *248*, 18-27.

[19] S. J. Freakley, Q. He, J. H. Harrhy, L. Lu, D. A. Crole, D. J. Morgan, E. N. Ntainjua, J. K. Edwards, A. F. Carley, A. Y. Borisevich, *Science* **2016**, *351*, 965-968.

[20] N. M. Wilson, D. W. Flaherty, *J. Am. Chem. Soc.* **2016**, *138*, 574-586.

[21] S. J. Freakley, M. Piccinini, J. K. Edwards, E. N. Ntainjua, J. A. Moulijn, G. J. Hutchings, *ACS Catal.* **2013**, *3*, 487-501.

[22] S. Shibata, T. Suenobu, S. Fukuzumi, *Angew. Chem. Int. Ed.* **2013**, *52*, 12327-12331.

[23] J. K. Edwards, E. Ntainjua, A. F. Carley, A. A. Herzing, C. J. Kiely, G. J. Hutchings, *Angew. Chem. Int. Ed.* **2009**, *48*, 8512-8515.

[24] S. Sterchele, P. Biasi, P. Centomo, S. Campestrini, A. Shchukarev, A.-R. Rautio, J.-P. Mikkola, T. Salmi, M. Zecca, *Catal. Today* **2015**, *248*, 40-47.

[25] S. Maity, M. Eswaramoorthy, *J. Mater. Chem. A* **2016**, *4*, 3233-3237.

[26] J. Li, K. Yoshizawa, *Catal. Today* **2015**, *248*, 142-148.

[27] A. Plauck, E. E. Stangland, J. A. Dumesic, M. Mavrikakis, *Proc. Natl. Acad. Sci. USA* **2016**, *113*, E1973-1982.

[28] W. B. Luo, X. W. Gao, S. L. Chou, J. Z. Wang, H. K. Liu, *Adv. Mater.* **2015**, *27*, 6862-6869.

[29] S. Zhang, O. Metin, D. Su, S. Sun, *Angew. Chem. Int. Ed.* **2013**, *52*, 3681-3684.

[30] N. Zheng, G. D. Stucky, *J. Am. Chem. Soc.* **2006**, *128*, 14278-14280.

[31] J. Zhang, Y. Li, Y. Zhang, M. Chen, L. Wang, C. Zhang, H. He, *Sci. Rep.* **2015**, *5*, 12950.

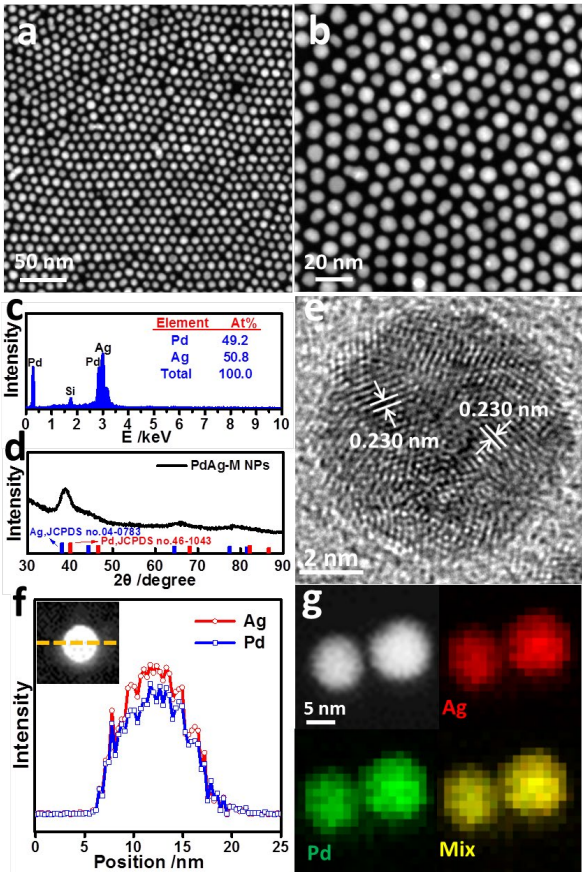

Figure 1. (a, b) HAADF-STEM images, (c) SEM-EDS spectrum, (d) XRD pattern, and (e) HRTEM image of the PdAg-M NPs. (f) STEM line scan analysis, and (g) HAADF-STEM image and corresponding element mappings of PdAg-M NPs.

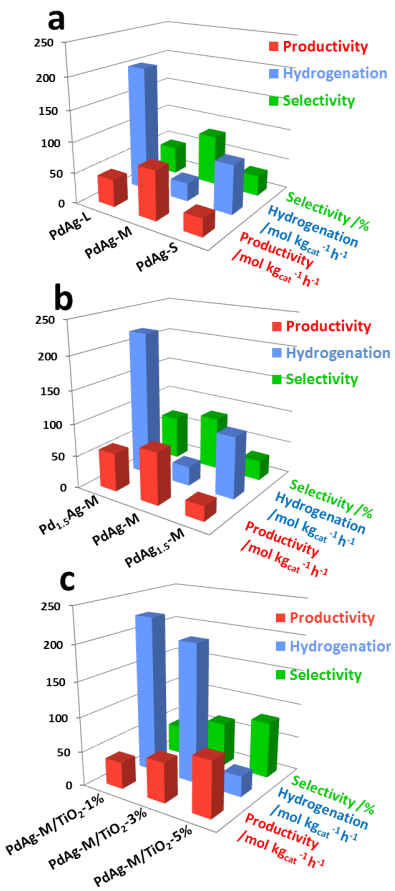

Figure 2. The catalytic performances of (a) Pd-Ag NPs with different sizes, (b) PdAg-M NPs with different component ratios, and (c) PdAg-M NPs/TiO_2 with different loadings.

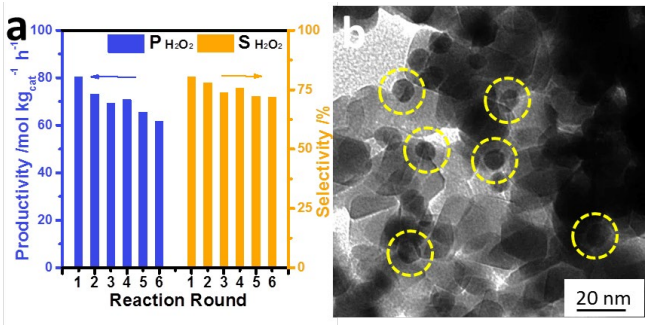

Figure 3. (a) The stability result of the PdAg-M for the direct H_2O_2 synthesis after six rounds. (b) TEM image of the PdAg-M NPs/TiO_2 after six rounds.

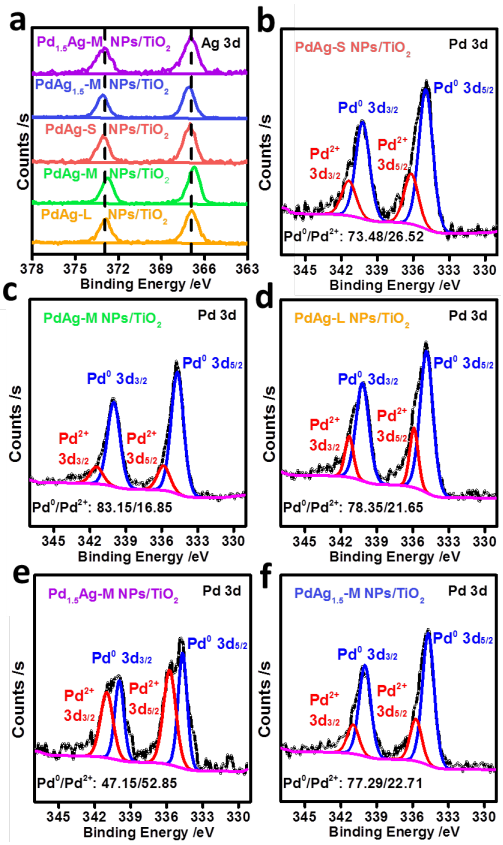

Figure 4. XPS curves of (a) Ag 3d and (b-f) Pd 3d with different Pd-Ag NPs.

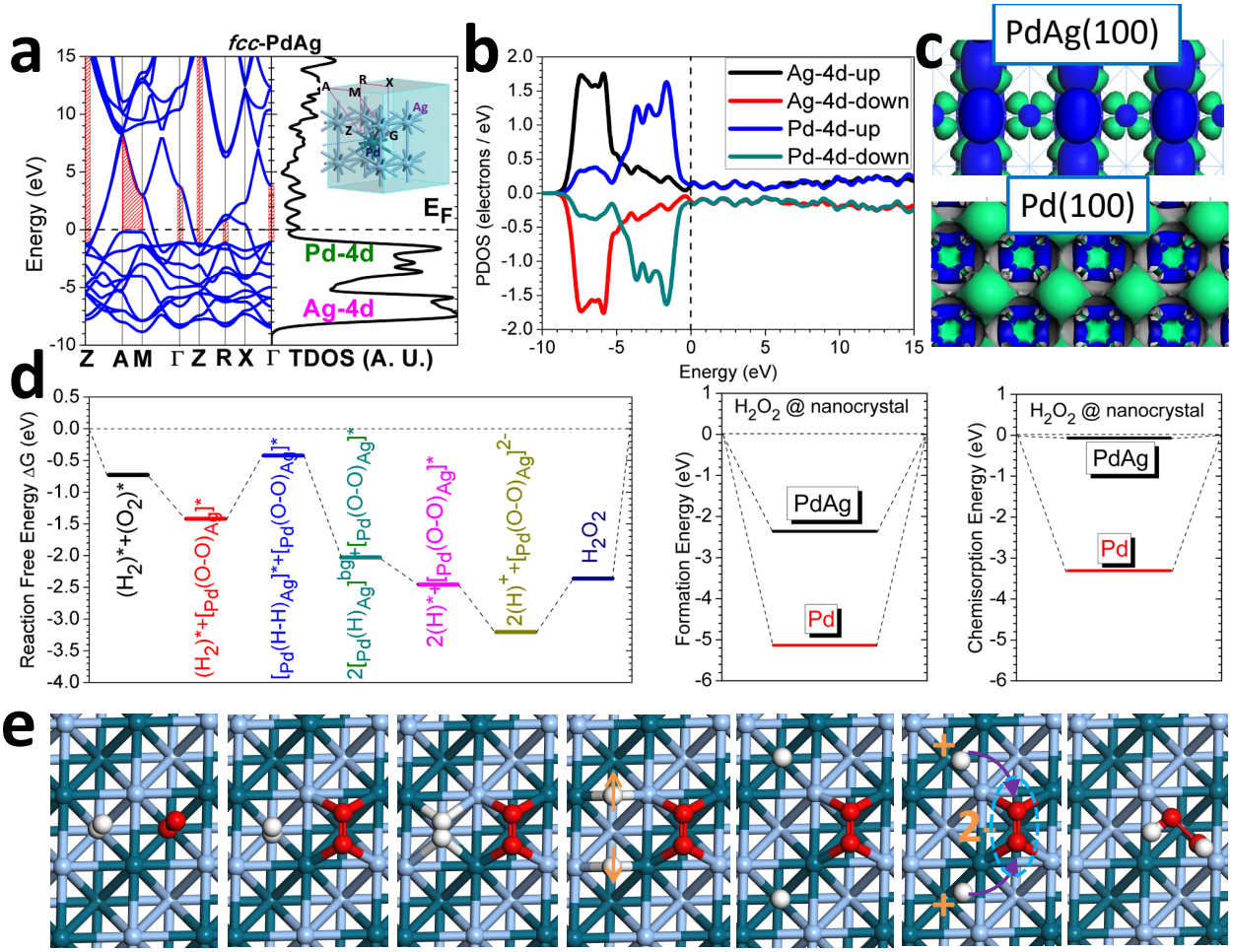

Figure 5. (a) The electronic band structure and total density of states (TDOS) of the primitive cell of *fcc*-PdAg model. The inserted figure is the reciprocal space of the *fcc*-PdAg. (b) The partial density of states (PDOS) of *fcc*-PdAg regarding the orbital level difference between Pd-4d and Ag-4d. (c) The 4d orbital real-spatial distribution on the PdAg (100) and Pd (100) with bonding and anti-bonding energy levels near E_F (0 eV). (d) The energy profile of the interpreted reaction regarding the reaction free energy (ΔG) simulated on the (100) surface of *fcc*-PdAg, formation energies of H_2O_2 on PdAg (100) and Pd (100), and the chemisorption energies of H_2O_2 on the PdAg (100) and Pd (100). (e) The local structures and bonding variations of H_2, O_2, and H_2O_2 in the simulation for interpreting the direct synthesis reaction (Pd=dark green, Ag=light blue, O=red, and H=white).